JOURNAL OF MATERIALS SCIENCE 30 (1995) 5607–5616

Fragmentation of aramid fibres in single-fibre model composites

M. C. ANDREWS, R. J. YOUNG
Manchester Materials Science Centre, UMIST/University of Manchester, Grosvenor Street, Manchester, M1 7HS, UK

Raman spectroscopy has been used to monitor the state of axial stress along fragmented, high-modulus Kevlar 149 aramid fibres in an epoxy resin matrix by monitoring the peak position of the strain-sensitive 1610 cm^{-1} aramid Raman band along individual fragments. It is shown that the interfacial shear stress along each fragment, derived from the strain-distribution profiles, is not constant as assumed by conventional fragmentation analysis. The fragmentation process of as-received Kevlar 149 fibres is compared to that of irradiated Kevlar 149 fibres exposed to ultraviolet light where the tensile strength and modulus of the fibres have been reduced. It is found that the derived interfacial shear stress and interfacial shear strength values are higher for those fibres exposed to ultraviolet light compared with the as-received fibres. It is also clearly demonstrated that the values of interfacial shear strength calculated at high matrix strains from conventional fragmentation analysis are considerably lower than the maximum value of interfacial shear stress prior to fibre fracture that was found to be close to the shear yield stress of the resin matrix. Hence the determination of the interfacial shear strength following the saturation of the fragmentation process may give rise to misleading results.

Nomenclature

e_f	Fibre strain
e_m	Matrix strain
e_f^{max}	Maximum strain along each fragment
e_f^*	Failure strain of the fibre
E_f	Fibre tensile modulus
l_c	Critical fragment length
$\langle l_c \rangle$	Mean critical fragment length
l_f	Fragment length
r	Fibre radius
x	Distance along the fibre
σ_f^{max}	Maximum stress along each fragment
σ_f^*	Fibre tensile strength
τ	Interfacial shear stress
τ_s	Interfacial shear strength

1. Introduction

Several micromechanical test methods have been developed to determine the interfacial properties of a composite by measuring the level of interfacial adhesion between a reinforcing fibre and a resin matrix. The methods developed more recently have been based upon the deformation of a single fibre partially or fully embedded in a resin matrix until failure of either the fibre, matrix or interface occurs. The most common methods include pull-out [1], microbond [2, 3], fragmentation [4] and microindentation [5] tests.

The level of interfacial adhesion is usually characterized by the interfacial shear strength parameter, τ_s, but is often calculated by making assumptions about material properties which may not give an accurate picture of the state of stress in the system. The complex state of stress due to the loading of the samples can often lead to variable, scattered results using conventional test techniques for the same fibre/matrix system [6].

In the fragmentation test, a single fibre is embedded in a dumb-bell specimen and aligned parallel to the tensile axis. The failure strain of the matrix should be at least three times the failure strain of the fibre. A stress is applied to the sample until failure of the fibre is observed either optically using polarized light [3, 7–9] or monitored indirectly by the use of acoustic emission [8]. Continued application of stress results in the progressive failure of the fibre at several points along its length until the fragments become so short that the shear stresses along their lengths can no longer build up enough tensile stresses to cause any further fracture. The interfacial shear strength, τ_s, can be calculated from

$$\tau_s = \frac{r\sigma_f^*}{l_c} \quad (1)$$

where r is the fibre radius, l_c is the critical fragment length and σ_f^* is the tensile strength the fibre at the critical length, l_c. Equation 1 simplifies the analysis of the fragmentation test in that debonding at the fragment ends is not accounted for and that the state of stress in each fragment is assumed to be uniform. This

0022–2461

is a very simplified approach which can lead to values of interfacial shear strength being underestimated.

The fibrillar fracture associated with aramid fibres make it difficult to determine the fragment length, l_f, using conventional techniques [3, 7–9] because the fractured region may extend axially along the fibre making it difficult to determine the point of fracture optically. An alternative method is to measure the acoustic emission signals generated by fibre fracture to determine the fragment length [8]. However, both optical and acoustic emission methods do not provide any information with respect to the stress in each fragment.

It has been shown that a Raman spectrum can be obtained from a high-modulus Kevlar 149 aramid fibre (Fig. 1) and that the strain-dependent shift of the 1610 cm^{-1} aramid Raman band (Fig. 2) can be used to determine the distribution of strain along aramid fibres embedded in an epoxy resin matrix [10–12]. The technique is extended here to analyse the distribution of fibre strain along a fragmented Kevlar 149 aramid fibre during a fragmentation test where the fragment length, l_f, can be determined. By monitoring the distribution of fibre strain at different loading levels it is shown that the interfacial shear stress, τ, can be derived at different matrix strains prior to, during, and following fibre fragmentation. The derived values of interfacial shear stress can be compared with the single value of interfacial shear strength, τ_s, calculated following saturation of fibre fracture using conventional analyses [3, 7–9].

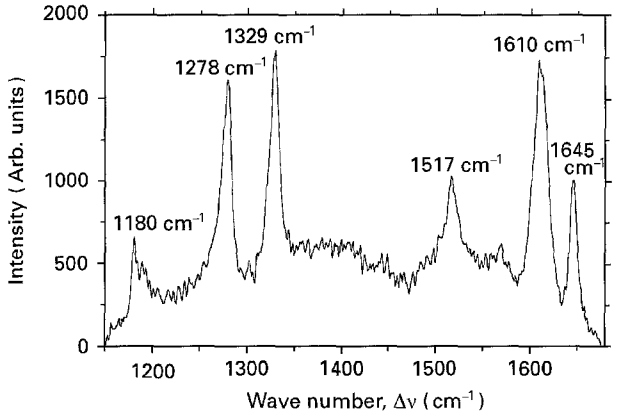

Figure 1 Raman spectrum of a Kevlar 149 fibre between 1100 and 1700 cm^{-1}.

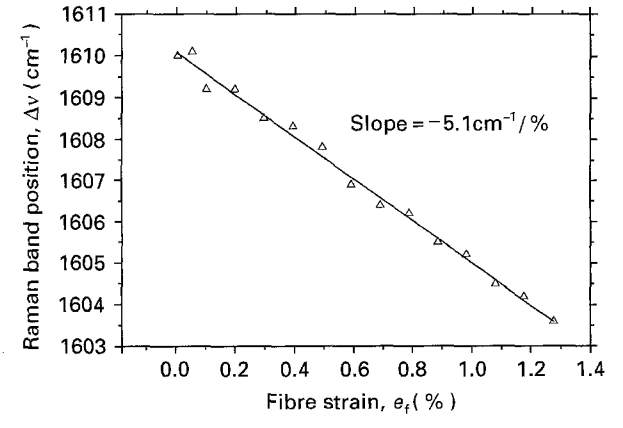

Figure 2 Dependence of the peak position of the 1610 cm^{-1} Raman band upon fibre strain for a Kevlar 149 fibre.

2. Experimental procedure

2.1. Materials and sample preparation

A commercial grade of aramid fibre, Kevlar 149, supplied by E.I. Du Pont de Nemours, Wilmington, USA was used in this study. The fibres were ~12 μm diameter with an initial fibre modulus, E_f, of 145 GPa and a failure strain, e_f^*, of 1.5%. Some of the Kevlar 149 fibres were exposed to a low-powered 15 W ultraviolet light source in a sealed light box for up to 5 weeks in order to reduce the tensile strength of the fibres [13]. The fibres, mounted on paper window cards, were turned over every 24 h. In this way the failure strain of the Kevlar 149 fibres was reduced to less than 1%, so that the failure strain of the epoxy resin matrix would be at least three times greater than that of the embedded fibres, as is normally required for fragmentation tests [3, 7–9].

Single short-fibre composite samples were prepared as shown schematically in Fig. 3. Kevlar 149 fibres were cut using ceramic scissors into small sections 2–4 mm long. The cut fibres were placed in a two-part cold-curing epoxy resin matrix consisting of 100 parts by weight LY5052 resin to 38 parts by weight HY5052 hardener supplied by Ciba Geigy. The samples were cured in a "picture frame" mould for 7 days at room temperature to avoid any residual thermal stresses in the composite samples. The resin composite was subsequently cut, shaped and polished to form dumb-bell shaped specimens ensuring that an aramid fibre was located in the central region parallel to the tensile axis.

The tensile behaviour of the resin matrix was also determined. Values of 3.1 GPa, 70 MPa and 4.1% were measured for the matrix tensile modulus, yield stress and failure strain, respectively. The compressive yield stress of the resin was found to be about 105 MPa which means that the shear yield stress of the matrix, τ_y, is about 43 MPa [14].

2.2. Raman spectroscopy

The single-fibre composite samples were mounted individually on a Miniature Materials straining rig, (Polymer Laboratories Ltd, UK). The strain in the matrix was measured using a strain gauge of gauge factor 2.09 bonded to the surface of the test region using a cold-curing slow-setting epoxy resin adhesive, as shown schematically in Fig. 3.

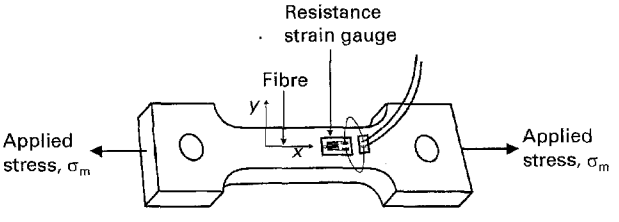

Figure 3 Schematic diagram of a single-fibre model composite.

The samples were placed on the stage of an Olympus BH-2 optical microscope connected via a set of collection optics to a Spex 1000M single monochromator. Raman spectra were obtained during deformation of the fibres in air and at regular intervals along the aramid fibres in the model composite samples, using the 632.8 nm red line of a 15 mW helium–neon laser focused to an ~5 μm spot on the surface of the fibre. A highly sensitive Wright Instruments charge-coupled device (CCD) camera cooled with liquid nitrogen was used to collect the Raman spectra using an exposure time of less than 10 s. For each sample, the peak position of the strain sensitive 1610 cm^{-1} Raman band [15, 16] was used to map the fibre strain distribution profiles along the length of the embedded fibres at matrix strains, e_m, from 0%–2.0% using small 10 μm steps close to the fibre ends.

3. Results and discussion

3.1. Stress transfer in a Kevlar 149 single-fibre model composite

The distribution of strain along the left-hand end of a single Kevlar 149 fibre in the epoxy resin matrix calculated from the point-to-point variation of the 1610 cm^{-1} aramid Raman band is shown in Fig. 4a. In the unstrained case, $e_m = 0\%$, there is virtually no strain in the fibre. As the matrix strain is increased the strain in the fibre increases from the fibre end up to a plateau strain value, along the middle of the fibre, approximately equal to the matrix strain. This behaviour is similar to that predicted by shear-lag theory [17]. However, unlike the behaviour predicted by shear-lag theory, the strain at the fibre end, $x = 0$ μm, is not equal to zero. This type of behaviour has also been reported for other aramid/epoxy systems [10–12, 18] and has been attributed largely to the geometry of the cut fibre end [19]. It is also shown that the solid lines in Fig. 4a, which are a fit of the experimental data to a logistic sigmoid function [10–12, 18], tend to smooth the experimental data particularly along the central region of the fibre. The scatter in the data could be attributed to either inaccuracies in the curve-fitting procedure used to determine the central peak position of the 1610 cm^{-1} Raman band or may represent locally stressed regions along the length of the fibre where fibre fracture may be initiated.

The interfacial shear stress, τ, can be derived using a force balance equilibrium [20] given by

$$\tau = E_f \frac{r}{2} \frac{de_f}{dx} \quad (2)$$

where de_f/dx is the differential of the variation of fibre strain with distance along the fibre calculated from the solid line fitted to the data in Fig. 4a. The variation of interfacial shear stress with distance, x, along the Kevlar 149 fibre in Fig. 4a is shown in Fig. 4b. At matrix strains up to 0.8% the interfacial shear stress is a maximum at the fibre end and decreases to zero at a distance, x, along the fibre. The interfacial shear stress at the fibre end reaches a maximum value of 42 MPa

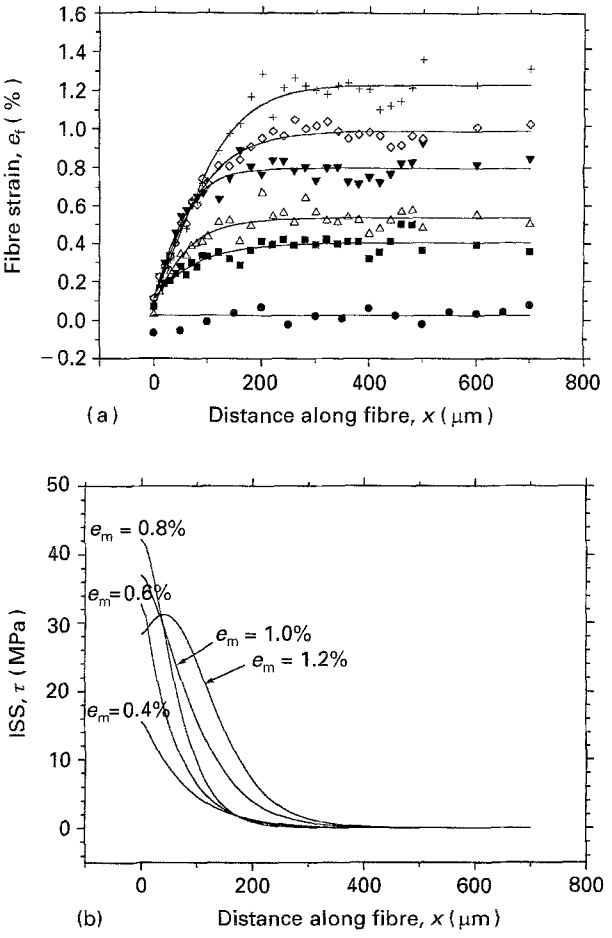

Figure 4 (a) Variation of fibre strain and (b) derived variation of interfacial shear stress, τ, with distance along the left-hand end of a Kevlar 149 fibre in a single-fibre model composite at different levels of matrix strain. (a) e_m; (●) 0%, (■) 0.4%, (△) 0.6%, (▼) 0.8%, (◇) 1.0%, (+) 1.2%.

where $e_m = 0.8\%$ and is close to the shear yield stress of the resin matrix. This behaviour has been repeatedly observed [10, 14, 18] for several aramid fibre/epoxy model composite systems and indicates that the maximum interfacial shear stress is highly dependent upon the mechanical properties of the epoxy resin matrix. Localized matrix yielding at the fibre/matrix interface causes the maximum value of interfacial shear stress to move along the fibre and can also initiate interfacial debonding close to the fibre end. This results in a reduction in the values of interfacial shear stress at the fibre end, as observed in Fig. 4b at 1.0% and 1.2% matrix strain.

3.2. Fragmentation of as-received Kevlar 149 fibres

Figs 5 and 6 show the distribution of fibre strain along the entire length of a Kevlar 149 fibre in a model composite at 0.5% and 1.0% matrix strain. At the low strain level, $e_m = 0.5\%$, the behaviour is similar to that predicted by shear-lag theory as was shown in Fig. 4a. It is shown, however, that the fibre strain fluctuates along the middle of the fibre. As discussed earlier, this may be due to the error in determining the peak position of the 1610 cm^{-1} aramid Raman band or may represent local variations in fibre strain along the

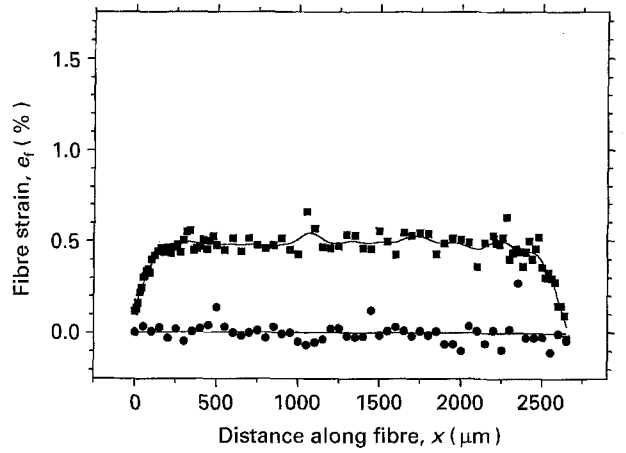

Figure 5 Variation of fibre strain along an as-received Kevlar 149 fibre in a single-fibre model composite at (●) 0% and (■) 0.5% strain.

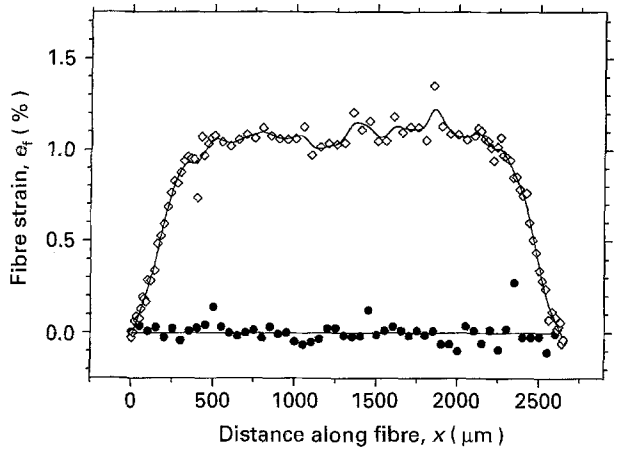

Figure 6 Variation of fibre strain along an as-received Kevlar 149 fibre in a single-fibre model composite at (●) 0% and (◇) 1.0% strain.

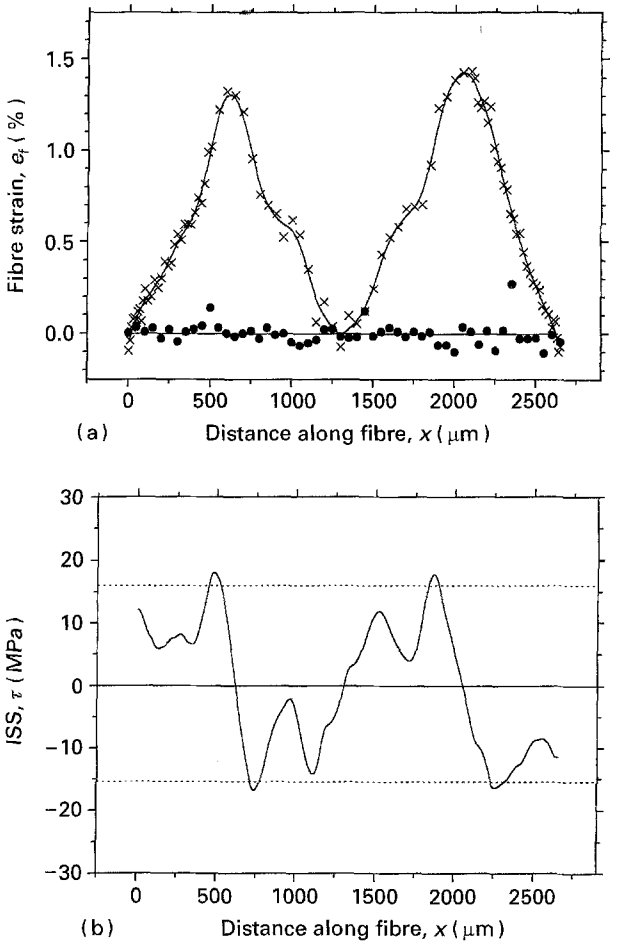

Figure 7 (a) Variation of fibre strain along an as-received Kevlar 149 fibre in a single-fibre model composite at (●) 0% and (×) 1.5% strain. (b) Derived variation of interfacial shear stress, τ, along an as-received Kevlar 149 fibre in a single-fibre model composite at 1.5% strain.

fibre. At 1.0% matrix strain the fibre strain distribution in Fig. 6 is trapezoidal due to yielding of the resin matrix close to the fibre ends [4, 21].

When the matrix strain is increased to 1.5% strain, as shown in Fig. 7a, the failure strain of the fibre is exceeded and fibre fracture occurs with the fibre breaking into two fragments. The fibre strain increases from the fibre ends in each of the fragments to a value of 1.4%, i.e. less than the matrix strain, at which point the fibre strain decreases. Increasing the matrix strain to 2.0% results in one of the fragments breaking into two smaller sections, shown in Fig. 8a. It is also shown that the maximum strain in each fragment has decreased even though the matrix strain has increased.

The solid lines in Figs 5, 6, 7a and 8a have been fitted using a cubic spline function [22]. This enables the variation of interfacial shear stress with distance, x, along the fibre to be derived accurately, using Equation 2. This is shown in Figs 7b and 8b for matrix strain levels of 1.5% and 2.0% where fibre fragmentation has occurred. When fibre fragmentation occurs, the interfacial shear stress distributions in Figs 7b and 8b become more complex than at low strains (Fig. 4b) with maximum values of interfacial shear stress located close to the fibre ends and at points of fracture along the fibre. The dotted lines in Figs 7b and 8b indicate the average values of maximum interfacial shear stress at the fibre and fragment ends.

It is apparent that the interfacial shear stress along each fragment is not constant as assumed by conventional fragmentation analysis [4] and presumed by Equation 1. Interfacial failure and localized matrix yielding at the interface can lead to non-linear distributions of fibre strain along the fibre fragments that are not expected by conventional fragmentation analysis which predicts that the distribution of fibre strain along each fragment should be approximately triangular.

3.3. Effect of ultraviolet light upon the tensile strength of Kevlar 149 aramid fibres

The strain to failure, e_f^*, of aramid fibres is relatively high compared with other high-performance fibres. The strain to failure of most aramid fibres is in excess of 2.5%. Therefore, most aramid fibres are unsuitable for studying fibre fragmentation in the present resin matrix where the failure strain is only 3–4%. The failure strain for the high-modulus fibre, Kevlar 149, is

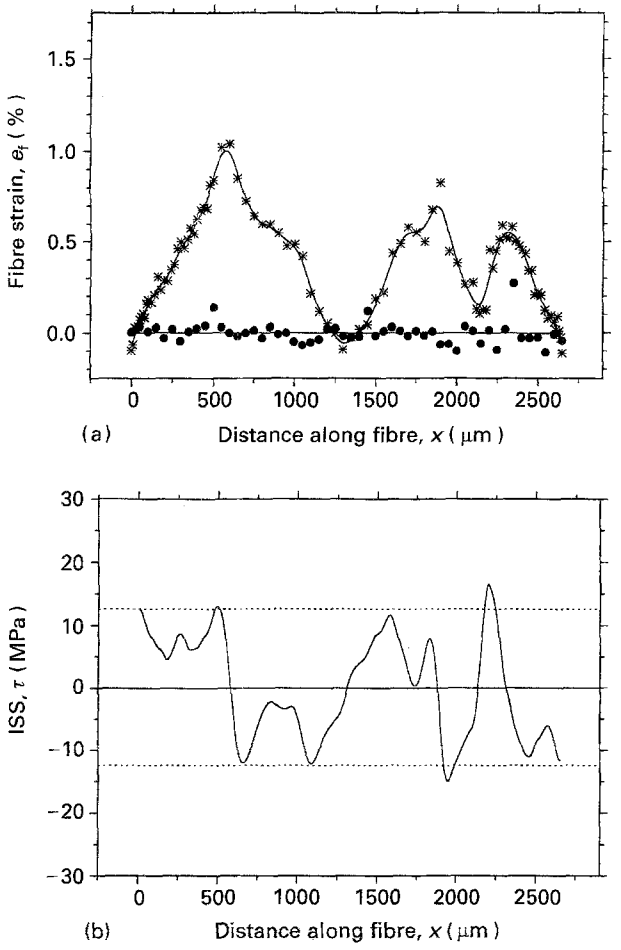

Figure 8 (a) Variation of fibre strain along an as-received Kevlar 149 fibre in a single-fibre model composite at (●) 0% and (*) 2.0% strain. (b) Derived variation of interfacial shear stress, τ, along an as-received Kevlar 149 fibre in a single-fibre model composite at 2.0% strain.

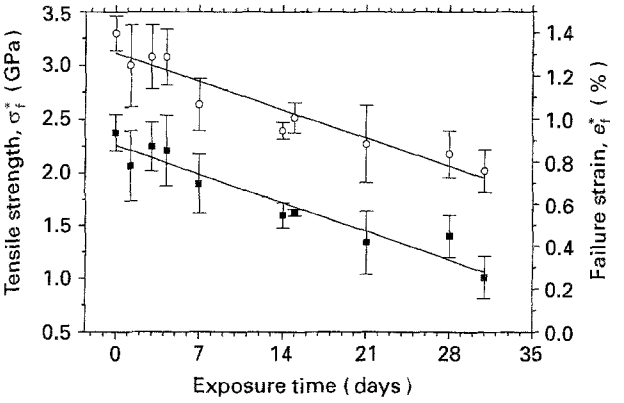

Figure 9 Effect of ultraviolet light upon the (■) tensile strength and (○) strain to failure of Kevlar 149 fibres.

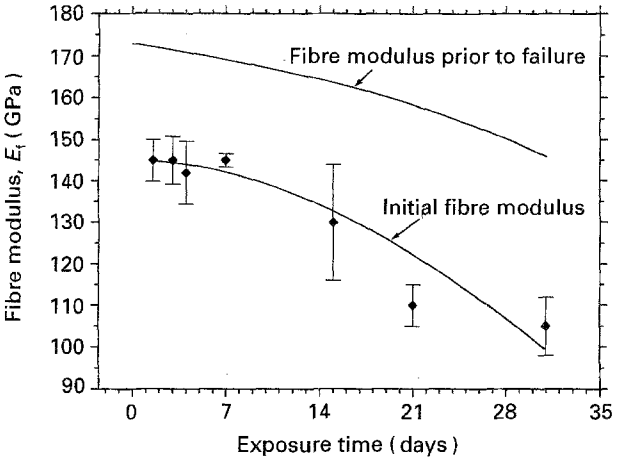

Figure 10 Effect of ultraviolet light upon the initial tensile modulus and the tensile modulus prior to failure of the Kevlar 149 fibres.

relatively low, $e_f^* < 1.5\%$, enabling a single-fibre model composite to be deformed in excess of the failure strain of the fibre.

The effect of ultraviolet radiation upon the tensile properties of aramid materials has been described previously [13, 23]. The aramid polymer degrades due to chain scission of the amide linkage in the polymer backbone [24].

The tensile properties of Kevlar 149 fibres exposed to a low-powered ultraviolet light source have been investigated in this present study. Fig. 9 shows the reduction in the tensile strength, σ_f^*, and the failure strain, e_f^*, for Kevlar 149 fibres exposed to ultraviolet light. A 50% reduction in both the tensile strength and strain to failure was observed following exposure of the Kevlar 149 fibres to the ultraviolet source for a period of 5 weeks. This was accompanied by a reduction in the initial fibre modulus and also the fibre modulus prior to tensile failure, as shown in Fig. 10. The tensile modulus prior to failure was determined from the tensile strength and strain to failure given by the solid lines in Fig. 9.

It is thought that wedge-shaped helical defects along the length of the unexposed as-received Kevlar 149 fibres, shown in Fig. 11, allow the ultraviolet light to penetrate into the centre of the fibre and make the

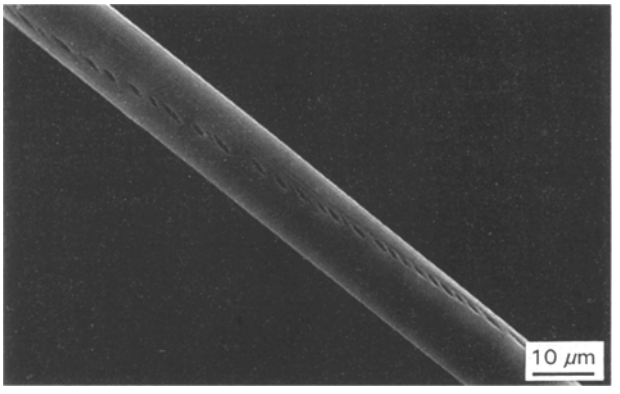

Figure 11 Scanning electron micrograph showing the wedge-shaped spiral defects along the length of an unexposed, as-received Kevlar 149 fibre.

fibres more susceptible to photodegradation compared with other aramid fibres [13] that do not possess such structural defects. The extensive damage caused by photodegradation results in a reduction of the tensile properties of the aramid fibres. The irradiated fibres fail in tension due to premature fibrillar fracture along the helical defect regions. The fibrillar regions between the wedge-shaped defects are prone to extensive damage. When this region is loaded in

tension, fibrillar fracture can occur that allows shearing or slippage to occur along the helical track and is thought to account for the reduction in the initial tensile modulus [13].

The effect of fibre degradation upon the fragmentation behaviour of irradiated Kevlar 149 fibres in model composites has been investigated and is developed next.

3.4. Fragmentation of Kevlar 149 fibres exposed to ultraviolet light

If fibre fracture occurs at low strain levels (less than 1%) the influence of localized matrix yielding and interfacial debonding [14, 18] upon the fragmentation process are reduced. This can be achieved by analysing the fragmentation process of the Kevlar 149 fibres exposed to ultraviolet light for 35 days where the strain to failure of the fibres has been reduced to less than 1.0%, as shown in Fig. 9. Figs 12, 13, 14a and 15a show the variation of fibre strain along an irradiated Kevlar 149 fibre in the epoxy resin matrix at different levels of matrix strain up to 2.0%. The distribution of fibre strain at 0.5% matrix strain is similar to that shown in Fig. 5 for the as-received fibre model composite. At 1.0% matrix strain (Fig. 13) initial fibre failure has occurred 1100 μm from the left-hand end of the fibre. Because the fibre strain at $x = 1100$ μm does not decrease to zero, it may be assumed that the crack has not propagated totally across the diameter of the fibre. As the matrix strain is increased to 1.5% (Fig. 14a) it can be seen that the fibre strain at $x = 1100$ μm has decreased to 0.25% indicating propagation of the crack across the fibre. It is also shown that further breaks have occurred randomly along the length of the fibre. This process continued until at 2.0% matrix strain (Fig. 15a) the fibre fragmented into a number of small fragments of length, l_f, in which the distribution of strain is approximately triangular. The maximum strain in each fragment, e_f^{max}, varies between 0.6% and 1.4% strain. It is evident that the maximum strain at different points along the fibre is much lower than the strain in the matrix. It therefore follows that the fibre in Fig. 15a is offering very little reinforcement.

The cubic splines fitted to the curves in Figs 14a and 15a have enabled the distribution of interfacial shear stress to be derived along the length of the fragmented fibre using Equation 2. The interfacial shear stress in

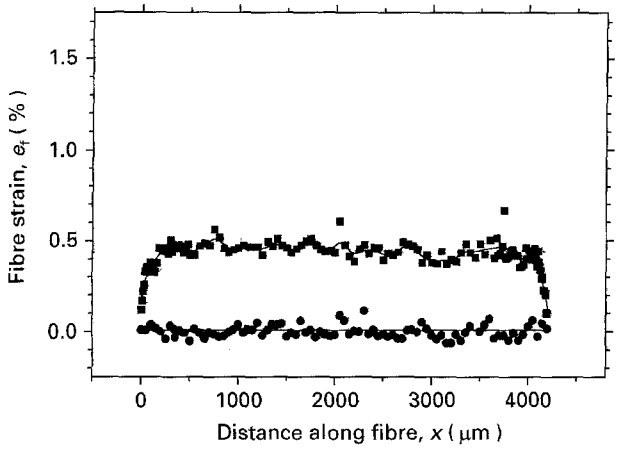

Figure 12 Variation of fibre strain along a Kevlar 149 fibre, exposed to ultraviolet light, in a single-fibre model composite at (●) 0% and (■) 0.5% strain.

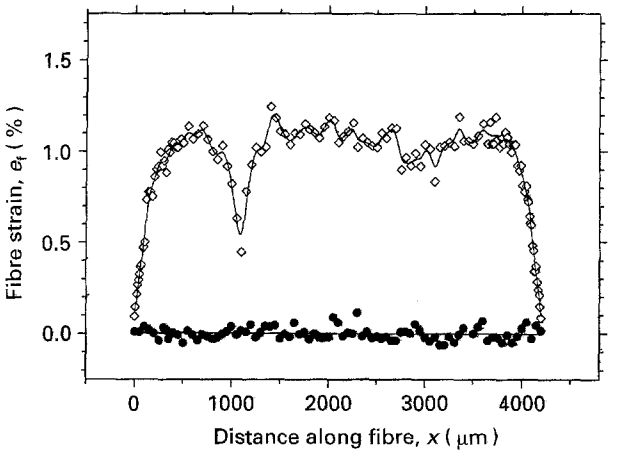

Figure 13 Variation of fibre strain along a Kevlar 149 fibre, exposed to ultraviolet light, in a single-fibre model composite at (●) 0% and (◇) 1.0% strain.

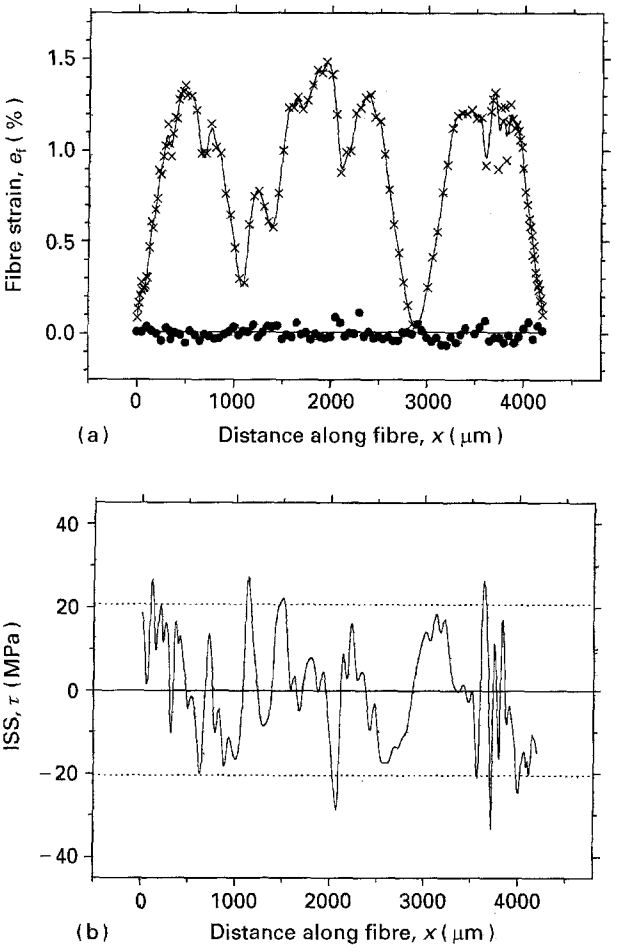

Figure 14 (a) Variation of fibre strain along a Kevlar 149 fibre, exposed to ultraviolet light, in a single-fibre model composite at (●) 0% and (×) 1.5% strain. (b) Derived variation of interfacial shear stress, τ, along a Kevlar 149 fibre, exposed to ultraviolet light, in a single-fibre model composite at 1.5% strain.

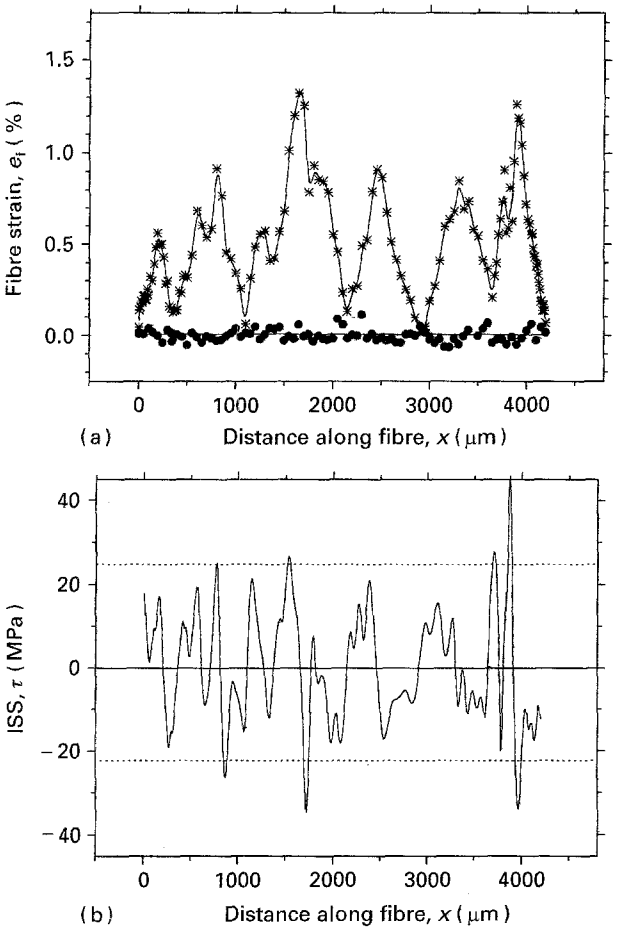

Figure 15 (a) Variation of fibre strain along a Kevlar 149 fibre, exposed to ultraviolet light, in a single-fibre model composite at (●) 0% and (*) 2.0% strain. (b) Derived variation of interfacial shear stress, τ, along a Kevlar 149 fibre, exposed to ultraviolet light, in a single-fibre model composite at 2.0% strain.

each fragment has a maximum value at the fragment ends. Along the middle of the fragments smaller peaks in interfacial shear stress can be observed that may be a result of partial fibrillar fracture along the fragment. The dotted lines in Figs 14b and 15b represent the mean value of maximum interfacial shear stress located at the fragment ends and is approximately equal to ±22 MPa. This is higher than the mean value of maximum interfacial shear stress for the as-received Kevlar 149 fibre system that was approximately equal to ±14 MPa as shown in Figs 7b and 8b. This implies that the irradiated fibres have better adhesion with the epoxy resin matrix than the as-received fibres. This may be possible if the free radicals generated during chain scission react to form oxidized chain ends that improve the chemical bonding at the fibre/matrix interface. The increased level of adhesion and reduction in tensile strength both lead to shorter fibre fragments in the case of the irradiated Kevlar 149 fibres. This can be seen in Table I where the fragment lengths for the as-received fibres are longer than those for the irradiated fibres.

3.5. Conventional fragmentation analysis

Conventional fragmentation procedures using either acoustic emission [8] or polarized light techniques [3, 7–9] rely upon the precise determination of the critical length fragment, l_c, in order to calculate the interfacial shear strength, τ_s, using Equation 1 [4]. This assumes that the shear stress along the interface is constant. It is shown in Fig. 15a that while the distribution of fibre strain along each fragment is approximately triangular, the interfacial shear stress in Fig. 15b, derived from the fitted curve in Fig. 15a, is by no means constant along each fragment. If the interfacial shear stress along each fragment is assumed to be constant, then the change in fibre strain along each fragment should be approximately linear thus forming a triangular fibre strain distribution along the length of the fibre. This is demonstrated in Fig. 16a where linear regression curves have been fitted to the strain distributions along each fragment in Fig. 15a. The variation of interfacial shear stress derived from the straight lines in Fig. 16a is shown in Fig. 16b. The uniform values of interfacial shear stress are approximately equal to ±10 MPa and are considerably lower than the values derived in Fig. 15b from the cubic spline curve fitted with greater accuracy to the same fibre strain distribution data.

If the critical fragment length, l_c, can be determined it is possible to determine a value of interfacial shear strength, τ_s, using Equation 1. The critical fragment length, l_c, is often underestimated if it is assumed to be equal to the fragment length, l_f. Towards the end of the fragmentation process, fragments in the range $l_c < l_f < 2l_c$ will continue to break to produce fragments in the range $l_c/2 < l_f < l_c$. Therefore, a uniform fragment length distribution is often assumed with a mean value $\langle l_c \rangle = 0.75 l_c$ [3, 7–9]. The interfacial shear strength is now given by

$$\tau_s = \frac{3}{4} \frac{r \sigma_f^*}{\langle l_c \rangle} \quad (3)$$

A better estimate of the mean critical fragment length can be obtained by using a Monte-Carlo simulation of a Poisson/Weibull probability model [25, 26] to represent the random occurrence of flaws along a fibre with a linear build up of the fibre tensile stress away from the fibre breaks.

Another problem associated with the conventional analysis is the determination of the tensile strength of the fibre at the critical fragment length because the fibre tensile strength usually increases as the fragment length decreases [27]. The value of fibre tensile strength is often calculated by measuring the tensile strength of the fibres with different gauge lengths (2–200 mm) and extrapolating back to find the tensile strength of the fibre at the critical fibre fragment length, l_c. Conventional analysis also assumes that the fibre strain at the point of fracture is equal to zero. This does not appear to be the case in Fig. 15a where the strain at the fragment ends is between 0% and 0.2%.

If the maximum stress in each fragment can be determined then the interfacial shear strength can be calculated by modifying Equation 1 to give

$$\tau_s = \frac{r \sigma_f^{\max}}{l_f} \quad (4)$$

TABLE I Values of interfacial shear strength for the as-received and irradiated Kevlar 149 fibres calculated from the individual fragment lengths, shown in Figs 7a, 8a and 15a, using Equation 4

Fibre	Matrix strain e_m (%)	Fragment length l_f (μm)	Maximum strain e_f^{max} (%)	Maximum stress σ_f^{max} (GPa)	Interfacial shear strength τ_s (MPa)
As-received Kevlar 149	Fig. 7a	1300	1.3	1.89	8.7
	$e_m = 1.5\%$	1250	1.5	2.18	10.7
	Fig. 8a	1300	1.0	1.45	6.7
	$e_m = 2.0\%$	810	0.7	1.02	7.6
		470	0.5	0.73	9.3
					Mean 8.6 (1.4)
Irradiated Kevlar 149	Fig. 15a	400	0.5	0.73	11.0
	$e_m = 2.0\%$	700	0.9	1.31	11.2
		1050	1.3	1.89	10.8
		750	0.9	1.31	10.5
		750	0.9	1.31	10.5
		550	1.2	1.74	18.9
					Mean 12.2 (3.1)

From the fibre strain distribution data in Figs 7a, 8a and 15a not only can the fragment length, l_f, be measured but also the maximum strain in each fragment, e_f^{max}, is known from which the maximum stress, σ_f^{max}, can be calculated. The interfacial shear strength, τ_s, can be calculated, using Equation 4, for each fragment shown in Figs 7a, 8a and 15a where there is well-defined saturated fragmentation. These values are given in Table I.

The mean interfacial shear strength, τ_s, was calculated using Equation 4 for both the as-received Kevlar 149 and irradiated Kevlar 149 single-fibre composite samples and the values are given in Table I. The mean value of interfacial shear strength of 12.2 MPa for the irradiated Kevlar 149 fibre is, as expected, close to the maximum values of interfacial shear stress, shown in Fig. 16b, derived from the triangular fibre strain distribution, shown in Fig. 16a, where the interfacial shear stress is assumed to be constant. It is also interesting to note that the mean interfacial shear strength of 12.2 MPa calculated for the irradiated Kevlar 149 sample is higher than the mean value of τ_s of 8.4 MPa calculated for the as-received Kevlar 149 fibre samples. This was also found to be the case for the values of interfacial shear stress derived from the Raman fibre strain distributions indicating that the irradiated fibres have better adhesion than the as-received fibres.

The mean values of interfacial shear stress, τ, and interfacial shear strength, τ_s, appear to be considerably lower than the values of maximum interfacial shear stress, τ_{max}, shown in Fig. 4b, calculated at low strain levels, $e_m \leqslant 1.2\%$ for an as-received Kevlar 149 model epoxy composite. This is clearly shown in Fig. 17 which gives the values of τ_{max} from Fig. 4b for the Kevlar 149 model composite together with the data calculated from fragmentation analysis. The circled data at 1.5% and 2.0% matrix shown in Fig. 17 indicate the mean values of maximum interfacial shear stress at the fragment ends indicated by the dotted lines in Figs 7b and 8b and Figs 14b and 15b for the as-received and irradiated Kevlar 149 fibres, respectively. The dotted lines in Fig. 17 indicate the mean

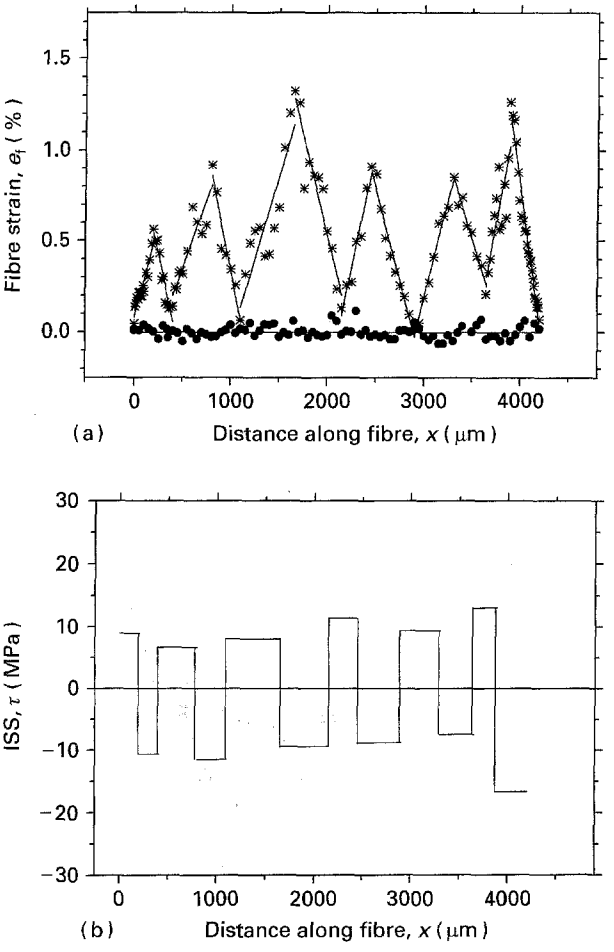

Figure 16 (a) Variation of fibre strain along the Kevlar 149 fibre exposed to ultraviolet light in Fig. 15a with linear regression lines fitted to the strain data along each fragment. e_m; (●) 0%, (*) 2.0%. (b) Variation of interfacial shear stress, τ, derived from the linear regression lines in (a) along the Kevlar 149 fibre exposed to ultraviolet light.

interfacial shear strength values shown in Table I calculated from Equation 4 using the conventional fragmentation analysis. The interfacial shear strength calculated from the fragmentation data was determined following fibre fracture which usually occurs after the

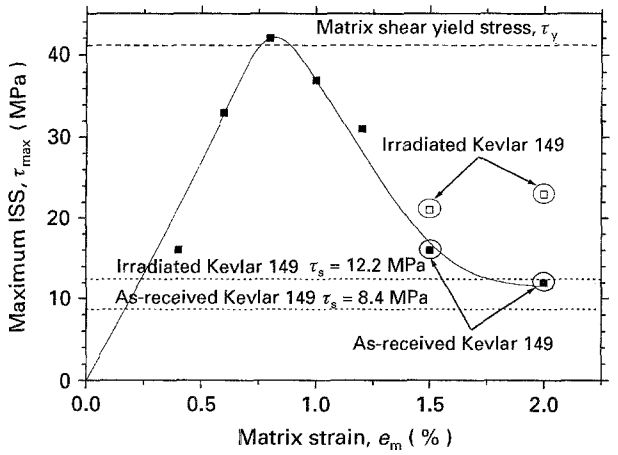

Figure 17 Dependence of maximum interfacial shear stress, τ_{max}, upon matrix strain for a Kevlar 149 fibre in a single-fibre model composite. (···) Values of interfacial shear strength, τ_s, calculated from the fragmentation data using Equation 4.

maximum value of interfacial shear stress has been attained. The maximum value of interfacial shear stress occurs prior to the onset of matrix yielding at the fibre/matrix interface [14, 18], i.e. when $e_m \sim 0.8\%$, after which point the value of τ_{max} decreases, as shown in Fig. 17. This indicates that the maximum interfacial shear stress is dependent upon the shear yield stress of the resin [14]. This is not apparent from the values of interfacial shear strength, τ_s calculated from the saturated fragmentation data which are calculated only at high strain levels.

The use of Raman spectroscopy to study the fracture of aramid fibres in a resin matrix has the advantage that the state of axial stress or strain can be clearly defined along the fragmented regions. This should be compared with conventional fragmentation techniques [3, 7–9] that do not give any direct measure of the state of stress in the fragments and in the case of aramids even the lengths of the fragments are difficult to measure. Using polarized light it is, however, possible to observe fragmented regions in a model composite and then map the distribution of strain along the fragments using Raman spectroscopy. This is demonstrated in Fig. 18 which shows the fibre strain distribution along the fragmented, irradiated Kevlar 149 fibre, shown in Fig. 15a, along with the birefringence pattern associated with fibre fracture in the same model composite viewed using polarized light. The problems associated with conventional fragmentation analysis discussed earlier, however, still remain.

4. Conclusions

It has been shown that Raman spectroscopy can be used to define clearly the axial strain-distribution profiles along fragmented aramid fibres from which the

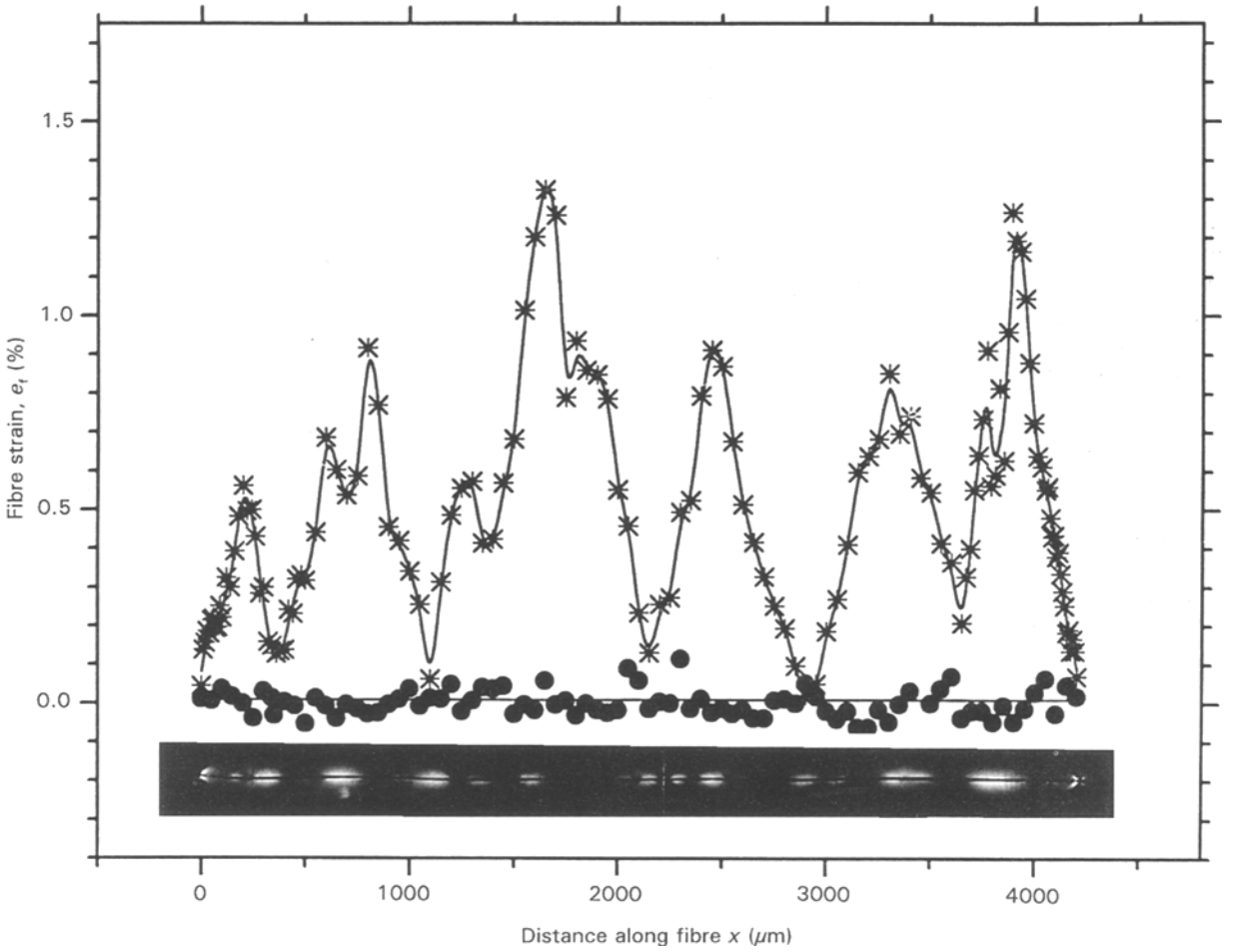

Figure 18 Variation of fibre strain along the Kevlar 149 fibre in Fig. 15a, exposed to ultraviolet light, in a single-fibre model composite at (●) 0% and (*) 2.0% strain and inset an optical micrograph of the same sample viewed under cross-polarized light.

interfacial shear stress can be derived accurately. It was found that the values of interfacial shear stress, τ, and interfacial shear strength, τ_s, were higher for the Kevlar 149 fibres exposed to ultraviolet light and may be a result of additional interfacial interactions between oxidized chain ends, formed by the reaction of free radicals generated during chain scission, and the epoxy resin matrix.

Using the Raman technique it is shown that each fragment length can be measured from the strain distribution profiles that would otherwise be difficult using conventional polarized light methods due to the fibrillar fracture associated with aramid fibres.

Determination of the interfacial properties of aramid fibres in an epoxy resin matrix using conventional fragmentation methods and analyses is usually difficult, because the fragment length and tensile strength of the fragment cannot be easily determined. It is also apparent that the assumption of constant interfacial shear stress is too simplified in the conventional analysis and may not be appropriate. This is because the values of interfacial shear strength calculated at high matrix strains following fibre fracture are considerably lower than the maximum value of interfacial shear stress calculated prior to fragmentation. This was found to be close to the shear yield stress of the epoxy resin matrix. This implies that interfacial failure is controlled by yielding of the epoxy resin matrix at the fibre/matrix interface and occurs well before the fragmentation process saturates. Hence great care must be exercised in the determination of interfacial parameters using conventional fragmentation analysis in the "saturated" state, because interfacial failure may have occurred at significantly lower levels of matrix strain.

Acknowledgements

This work was supported by a Research Grant from the Science and Engineering Research Council and the Ministry of Defence. The authors thank E.I. Du Pont de Nemours for supplying the aramid fibres used in this study. R. J. Y. thanks the Royal Society for support in the form of the Wolfson Research Professorship in Materials Science.

References

1. L. J. BROUTMANN, "Interfaces in Composites", ASTM STP 452 (American Society for Testing and Materials, Philadelphia, PA, 1969) p. 27.
2. B. MILLER, P. MURI and L. REBENFELD, *Compos. Sci. Technol.* **28** (1987) 17.
3. P. J. HERRERA-FRANCO and L. T. DRZAL, *Composites* **23** (1992) 2.
4. A. KELLY and W. R. TYSON, *J. Mech. Phys. Solids* **13** (1965) 329.
5. J. F. MANDELL, D. H. GRANDE, T. H. TSIANG and F. J. McGARRY, in "Composite Materials Testing and Design" (Seventh Conference), ASTM STP 893, edited by J. M. Whitney (American Society for Testing and Materials, Philadelphia, PA, 1986) p. 87.
6. M. J. PITKETHLY, J. P. FAVRE, U. GAUR, J. JAKUBOWSKI, S. F. MUDRICH, D. L. CALDWELL, L. T. DRZAL, M. NARDIN, H. D. WAGNER, L. DI LANDRO, A. HAMPE, J. P. ARMISTEAD, M. DESAEGER and I. VERPOEST, *Compos. Sci. Technol.* **48** (1993) 205.
7. H. D. WAGNER, H. E. GALLIS and E. WIESEL, *J. Mater. Sci.* **28** (1993) 2238.
8. A. N. NETRAVALI, Z-F LI, W. SACHSE and H. F. WU, *ibid.* **28** (1991) 6631.
9. J. KALANTAR and L. T. DRZAL, *ibid.* **25** (1990) 4194.
10. M. C. ANDREWS and R. J. YOUNG, *Mater. Sci. Eng.* **A184** (1994) 197.
11. M. C. ANDREWS and R. J. YOUNG, *J. Raman Spectrosc.* **24** (1993) 539.
12. M. C. ANDREWS, R. J. DAY, A. K. PATRIKIS and R. J. YOUNG, *Composites* **25** (1994) 745.
13. M. G. DOBB, R. M. ROBSON and A. H. ROBERTS, *J. Mater. Sci.* **28** (1993) 785.
14. M. C. ANDREWS, R. J. YOUNG and R. J. DAY, in "Developments in the Science and Technology of Composite Materials", edited by A. R. Bunsell, A. Kelly and A. Massiah (Woodhead, Cambridge, 1993) p. 133.
15. S. VAN DER ZWAAG, M. G. NORTHOLT, R. J. YOUNG, I. M. ROBINSON, C. GALIOTIS and D. N. BATCHELDER, *Polym. Commun.* **28** (1987) 276.
16. C. CHANG and S. L. HSU, *Macromolecules* **23** (1990) 1484.
17. H. L. COX, *J. Appl. Phys.* **3** (1952) 72.
18. M. C. ANDREWS, R. J. YOUNG and J. MAHY, *Compos. Interfaces*, **2** (1994) 433.
19. C. F. FAN and S. L. HSU, *Macromolecules* **22** (1989) 1474.
20. A. KELLY and N. H. MacMILLAN, "Strong Solids", 3rd Edn (Clarendon Press, Oxford, 1986).
21. M. R. PIGGOTT, "Load Bearing Fibre Composites" (Pergamon, Oxford, 1980) p. 83.
22. C. H. REINSCH, *Numer. Math.* **10** (1967) 177.
23. S. C. POWELL, R. L. KIEFER, P. L. PATE and R. A. ORWOLL, *Polym. Prep.* **32** (1991) 122.
24. D. J. CARLSSON, L. H. GAN and D. M. WILES, *J. Polym. Sci. A. Polym. Chem.* **16** (1978) 2353.
25. W. F. KNOFF, *J. Mater. Sci.* **28** (1993) 931.
26. R. B. HENSTENBERG and S. L. PHOENIX, *Polym Compos.* **10** (1989) 385.
27. S. A. FAWAZ, A. N. PALAZOTTO and C. S. WANG, *Polymer* **33** (1992) 100.

Received 22 December 1994
and accepted 15 March 1995